Fiscaletti, D., & Ganapathisubramani, B. (2018). Characteristics of sources and sinks of momentum in a turbulent boundary layer. *Physical Review Fluids*, *3*(054601). https://doi.org/10.1103/PhysRevFluids.3.054601

Characteristics of sources and sinks of momentum in a turbulent boundary layer

D. Fiscaletti[1,2,*] and B. Ganapathisubramani[1]

[1]*Engineering and the Environment, University of Southampton, Southampton SO17 1BJ, United Kingdom*

[2]*Department of Aerospace Engineering, University of Bristol, Bristol BS8 1TR, United Kingdom*

(Received 17 January 2018; published 3 May 2018)

In turbulent boundary layers, the wall-normal gradient of the Reynolds shear stress identifies momentum sources and sinks ($T = \partial[-uv]/\partial y$). These motions can be physically interpreted in two ways: (1) as contributors to the turbulence term balancing the mean momentum equation, and (2) as regions of strong local interaction between velocity and vorticity fluctuations. In this paper, the space-time evolution of momentum sources and sinks is investigated in a turbulent boundary layer at the Reynolds number (Re_τ) = 2700, with time-resolved planar particle image velocimetry in a plane along the streamwise and wall-normal directions. Wave number-frequency power spectra of T fluctuations reveal that the wave velocities of momentum sources and sinks tend to match the local streamwise velocity in proximity to the wall. However, as the distance from the wall increases, the wave velocities of the T events are slightly lower than the local streamwise velocities of the flow, which is also confirmed from the tracking in time of the intense momentum sources and sinks. This evidences that momentum sources and sinks are preferentially located in low-momentum regions of the flow. The spectral content of the T fluctuations is maximum at the wall, but it decreases monotonically as the distance from the wall grows. The relative spectral contributions of the different wavelengths remains unaltered at varying wall-normal locations. From autocorrelation coefficient maps, the characteristic streamwise and wall-normal extents of the T motions are respectively 60 and 40 wall units, independent of the wall distance. Both statistics and instantaneous visualizations show that momentum sources and sinks have a preferential tendency to be organized in positive-negative pairs in the wall-normal direction.

DOI: 10.1103/PhysRevFluids.3.054601

I. INTRODUCTION

Several flow structures have been investigated that play a significant role in the Reynolds stress production and in transport of mass and momentum, in wall-bounded flows. These features include hairpin vortices [1,2] and packet of vortices [3,4], ejections and sweeps [5,6], and large-scale motions [7–10]. Nonetheless, the mean momentum equation shows that the gradient of Reynolds shear stress is highly relevant to the rate of change of momentum. The mean momentum equation for a zero-pressure-gradient turbulent boundary layer (TBL) is

$$U\frac{\partial U}{\partial x} + V\frac{\partial U}{\partial y} = \nu\frac{\partial^2 U}{\partial y^2} + \overline{T}, \tag{1}$$

*Corresponding author: d.fiscaletti@bristol.ac.uk

where

$$T = \frac{\partial(-uv)}{\partial y}. \tag{2}$$

In this formulation of the mean momentum equation and throughout this paper, the streamwise, wall-normal, and spanwise directions are along the x, y, and z axes. The mean and fluctuating velocity components along these three directions are respectively given by (U, V, W) and (u, v, w). Kinematic viscosity of the fluid is ν. The overline represents the operation of averaging in time. In Eq. (1) the terms on the left-hand side of the equal represent mean advection, which is balanced by the terms on the right-hand side of the equals sign. The term $\nu \frac{\partial^2 U}{\partial y^2}$ represents physically the momentum transport at a molecular level, while the term $\overline{T}$ is the mean momentum transport induced by the fluctuating velocity field, thus by turbulence. The present work focuses on the term T of the mean momentum equation. This is dimensionally a forcelike quantity, and it can act as a sink or a source of momentum depending on its sign. In other words, the term T accounts for the action of turbulence in balancing the rate of change of momentum expressed in Eq. (1).

When examining the value of the term $\overline{T}$ at different wall-normal positions, a four-layer structure could be identified for different wall-bounded flows, as shown by Refs. [11,12]. The relative weight of $\overline{T}$ over the viscous term was quantified from both experimental and direct numerical simulations data and used to the explain dynamical properties of each layer. These empirical observations on the wall-normal gradient of the Reynolds shear stress provided the basis for an alternative physical model of the TBL, which was proposed in Ref. [13]. According to this model, the relative magnitude of $\overline{T}$ over the viscous term can be associated with the dynamics of the vortical motions examined in earlier studies. In this way, a link could be established between the hairpin paradigm and the observed four-layer structure. In this respect, it can also be shown mathematically that velocity and vorticity fluctuations can be related to the Reynolds shear stress gradient as

$$\overline{T} = \overline{[\boldsymbol{u} \times \boldsymbol{\omega}]_x} + \frac{1}{2}\frac{\partial}{\partial x}(\overline{v^2} + \overline{w^2} - \overline{u^2}), \tag{3}$$

where $[\boldsymbol{u} \times \boldsymbol{\omega}]_x = v\omega_z - w\omega_y$, and $(\omega_x, \omega_y, \omega_z)$ are the fluctuations of the vorticity along the x, y, and z axes. In a turbulent channel flow, the last term of Eq. (3) is zero, while in TBLs that term is generally small [14]. Therefore, for a TBL, Eq. (3) simplifies as

$$\overline{T} \approx \overline{v\omega_z} - \overline{w\omega_y}. \tag{4}$$

This simplification for Eq. (3) enabled Ref. [15] to estimate terms $\overline{v\omega_z}$ and $\overline{w\omega_y}$, and their contributions to $\overline{T}$, from hot-wire anemometry measurements in a channel flow. These results were later confirmed by the studies of Refs. [16] and [17], respectively, from simulations and experiments.

The direct relationship between $[\boldsymbol{u} \times \boldsymbol{\omega}]_x$ and momentum sources and sinks, which is described by Eq. (3), motivated further investigations of the velocity-vorticity interactions after the pioneering measurements in Ref. [15]. The authors of Ref. [18] examined the structure of the velocity field associated with the spanwise vorticity field and presented one-point correlations of $v\omega_z$ and $w\omega_y$. These correlations suggested the presence of internal layers of intense shear, inclined to the wall. The authors of Ref. [19] studied the velocity-vorticity interactions in the near-wall region of a TBL at a low Reynolds number. The dynamics of the coherent structures of vorticity in relation to ejections and sweeps were associated with the gradient of the Reynolds stress.

The spectral content of the velocity-vorticity interactions could be quantified from cospectra in a TBL, using hot-wire anemometry measurements [20]. In particular, the effects of both Reynolds number and wall roughness were explored. It was found that the statistics of $v\omega_z$ and its cospectrum are considerably sensitive to wall roughness as well as to the Reynolds number of the flow. The low-wave number peak in the velocity-vorticity cospectra and earlier observations over the spatial organization of hairpin packets of vortices led to elaborating a conceptual scenario illustrating the general structure of TBLs. According to this, large-scale regions of approximately uniform streamwise momentum

are surrounded by elongated "fissures" of highly vortical flow. Later observations based on particle image velocimetry (PIV) confirmed and highlighted the importance of this interpretation [21,22].

The authors of Ref. [23] computed the wall-normal derivative of the uv cospectra in the outer region of a pipe flow, at different distances from the wall. They observed that the very-large-scale motions within the flow contribute significantly to the wall-normal gradient of the Reynolds shear stress. In particular, the contribution associated with the very large-scale motions is comparable to that from smaller motions, including the large-scale motions. The authors of Ref. [24] examined velocity-vorticity correlations in a turbulent channel flow, from direct numerical simulations. These correlations rapidly change behavior when moving from the wall up to the location where the Reynolds shear stress is maximum, while beyond this point their behavior is not significantly altered. A mild asymmetry in the velocity-vorticity correlations along the streamwise direction was regarded as responsible for the nonzero mean of the Reynolds shear stress gradient, which balances the mean momentum equations. It was concluded that a subtle deviation from the asymmetry in the velocity-vorticity correlations implies large changes in the mean velocity flow.

The spatial organization and statistical structure of momentum sources and sinks was investigated in Ref. [25], at two different wall-normal positions. PIV data were acquired in streamwise-spanwise planes. It was obtained that the size of momentum sources remains relatively constant across the two wall-normal locations under analysis, whereas the size of momentum sinks increases with the wall distance. Both momentum sources and sinks are located in low-velocity regions of the flow. The sign of the velocity fluctuations changes in the vicinity of sinks, which implies a transition between quadrants.

Thus far, the spectral content of the Reynolds shear stress gradient [T term, Eq. (2)] has been investigated based on cospectra of the velocity-vorticity fluctuations. In this way, the spectral composition of $v\omega_z$ and $w\omega_y$ was derived, and therefore of T. However, the spectral content of the motions constituting T is still unknown, in that the spectral composition of the T fluctuations has never been examined. In the present work, wave number-frequency power spectra of the T fluctuations are presented. The characteristic wave velocity of the T events is estimated at different wall-normal locations, which to our knowledge has not been assessed previously.

In the past, the size and spatial organization of Reynolds shear stress structure have been examined only at two wall-normal locations and along the streamwise-spanwise directions [25]. As a consequence, it is still obscure how momentum sources and sinks are spatially organized in the wall-normal direction, and what is their characteristic size, also in relation to their wall distance. With the aim of quantifying size and spatial distribution of momentum sources and sinks, here autocorrelation coefficient maps are calculated. In addition, intense T events are identified with an approach similar to that of Ref. [26] and tracked in time. The local velocities of the intense T events are estimated at different wall distances and compared to the wave velocity obtained from spectra.

II. EXPERIMENTS AND METHODS OF ANALYSIS

In the present work, time-resolved PIV velocity fields of a TBL are analyzed. A brief summary of the data set is given in the following discussion, and further details about the experimental campaign can be found in Refs. [27,28]. The data set itself is also openly available at Ref. [29].

The TBL data set consists of time-resolved PIV data in a plane along the streamwise and wall-normal directions. Nominal flow conditions at the measurement location (4.5 m downstream of a glass rod trip) in the water tunnel were free-stream velocity, $U_\infty = 0.67$ m s^{-1}; boundary layer thickness, $\delta = 0.1$ m; friction velocity, $U_\tau = 0.027$ m s^{-1}; and corresponding Reynolds number, $\mathrm{Re}_\tau = 2700$. Four high-speed cameras were placed side by side with the aim of obtaining a field of view (FOV) of an adequate streamwise dimension. Each camera's FOV was calibrated using a single calibration plate, which covered the full FOV of the measurement.

Particle images are acquired and analyzed using the LaVision software DaVis 7.2. A min-max normalization was applied to the PIV images before processing. Gaussian-weighted correlation with a hierarchical approach started with an initial window size of 64 × 64 pixels and finished at 16 × 16

pixels, with an overlap factor of 50%. The resulting data covered an area of 0.185 m × 0.045 m (1.185 $\delta \times 0.45\,\delta$). The spatial resolution of the data was $h^+ = 10$, and the temporal resolution was $tU_\tau^2/\nu = 0.7$. About 50 000 velocity fields were obtained in total—10 runs of 5000 images over 5 s each—for a time span larger than 300 δ/U_∞.

A. Methods for identification and tracking in time of intense T events

The main subjects of the present investigation are the intense momentum sources and sinks that populate the TBL. They are detected and statistically characterized in terms of extension, average intensity, and position of their weighted centroids. From the time-resolved data, the events are tracked across the time, which enables us to obtain the instantaneous local velocities of each event. In this section, we describe the method used for detecting and time tracking the intense T events.

The noise in the PIV data was attenuated *a posteriori* by applying a regression filter, before calculating the Reynolds stress gradient. The filtering of the data was performed both in time and in space, similar to the procedure in Ref. [28]. The filter replaces the value measured experimentally in a certain point of the domain, with the value obtained in the same point by least-square fitting a polynomial function of the second order in x (streamwise direction) and y (wall-normal direction), and of the first order in the third dimension (time), in a $5 \times 5 \times 3$ neighborhood around the point. Details on this regression filter are given in Ref. [30]. From these filtered velocity vector fields we obtained the instantaneous Reynolds shear stress fields (uv). The discrete derivative of uv over the wall-normal direction, which was computed with a second-order central difference scheme, enabled us to compute T fields. Similarly, fields of $v\omega_z$ were also obtained.

The criterion used for the detection of the intense T events is analogous to that in Ref. [26] and is the following:

$$|T(x,y)| > H\,T_{\mathrm{rms}}(y)\big|_{\mathrm{max}}, \tag{5}$$

where $T_{\mathrm{rms}}(y)\big|_{\mathrm{max}} = 1.5\,(\mathrm{m/s^2})$ is the maximum of $T_{\mathrm{rms}}(y)$ across the range of wall-normal locations available from experiments, and H is a coefficient. The maximum of $T_{\mathrm{rms}}(y)$ was obtained at the closest point to the wall ($y/\delta \approx 0.02$). Throughout the analysis, we adopted $H = 0.8$. In addition, the connected regions satisfying the criterion in Eq. (5) should be at least composed of nine points in order to be identified and tracked. In this way, transport events that are excessively small in size are discarded, as they can be the result of measurement error (spurious vectors or outliers [31]).

In the present section, the algorithm for the tracking of the intense intense momentum sources and sinks is described too. Two intense T events ev_1 and ev_2 that are identified at two consecutive time instants are considered to be the same event if the following relationship holds:

$$d_{\mathrm{cent}} < D_{\mathrm{box}}, \tag{6}$$

where d_{cent} is the distance between the centroids of ev_1 and ev_2, and D_{box} is the diagonal of the smallest rectangle including all points of ev_1. The same algorithm was used in Ref. [28] for tracking in time the intense Reynolds-shear-stress events. Further details on this algorithm can be found in Sec. II of that study.

The range of wall-normal locations, the object of the present study, falls partially within the logarithmic region of the turbulent boundary layer, and it extends farther, entering the wake region of the flow. Nonetheless, given that the results in the current work are presented in the context of momentum sources and sinks, the traditional classification of wall-normal locations based on logarithmic and wake layers may not be appropriate. The wall-normal locations examined in the following can be better classified based on the four-layer structure described by Ref. [11]. In this case, the wall-normal locations are partially in layer III, the viscous-advection balance mesolayer, and in layer IV, the inertial-advection balance layer. Specifically, layer III ranges from $y^+ \approx 1.6 \times (\mathrm{Re}_\tau)^{1/2}$ to $y^+ \approx 2.6 \times (\mathrm{Re}_\tau)^{1/2}$, and layer IV ranges from $y^+ \approx 2.6 \times (\mathrm{Re}_\tau)^{1/2}$ to $y^+ = \mathrm{Re}_\tau$ (see Ref. [11], p. 308, section 2.2 for details on the physical extent of the four layers).

III. RESULTS AND DISCUSSION

From the time-resolved fields of T, the inner-normalized mean profile $\overline{T}^+$ could be calculated, and it is given in Fig. 1. The inner-normalized mean profile of $\overline{v\omega_z}^+$ is also reported in Fig. 1. The relationship between $\overline{v\omega_z}$ and $\overline{T}$ is shown in Eq. (4). The largest value of $\overline{T}^+$ is obtained at the lowest wall-normal location available from the measurements (close to the wall). At increasing wall distance, $\overline{T}^+$ rapidly decreases and becomes negative. Therefore, a local maximum of the $-\overline{uv}$ profile ($\overline{T} = 0$) is obtained at $y^+ \approx 140$. At $y^+ > 140$, we obtained $\overline{T}^+ < 0$ independent of wall-normal position. The profile of $\overline{T}$ presented in Fig. 1 agrees well with the experimental study of Ref. [24] (their Fig. 1). In this range of wall-normal locations, a prevalence of momentum sinks is in agreement with the growth of $\overline{uv}$ for increasing y^+. The $\overline{v\omega_z}^+$ profile exhibits its smallest value at the lowest wall-normal location of the measurement FOV (close to the wall). Throughout the examined range of wall-normal locations, $\overline{v\omega_z}^+$ remains negative, which is evidence that positive wall-normal velocity fluctuations tend to be associated with negative out-of-plane vorticity fluctuations (clockwise-rotating vortices), whereas negative wall-normal velocity fluctuations are with positive out-of-plane vorticity fluctuations (counterclockwise-rotating vortices). The $\overline{v\omega_z}^+$ profile shown in Fig. 1 is analogous to that presented in Ref. [15] (Fig. 1 of that work) and more recently in Ref. [24]. After reporting the mean profile of the Reynolds shear stress gradient, it is of interest to examine the motions that contribute to this mean value. The characteristics of the T motions can be assessed by determining the spectral content of the T fluctuations, the size and spatial organization of the T events, and their local velocities.

In Fig. 2 the wave number-frequency power spectra of the T fluctuations (P_T) are presented in a logarithmic scale, at different wall-normal distances. The continuous blue lines indicate the mean streamwise velocity of the flow. From the analysis of the spectra, T events are characterized by the largest spectral content in proximity to the wall, while at increasing wall-normal locations their spectral content gradually diminishes. This can be appreciated from the range of shades in the wave number-frequency power spectrum, in which the maximum value decreases progressively at growing wall-normal locations. Another consequence of the decrease in the spectral content associated with the T events at growing wall-normal locations is that the extension of the visible region of the power spectrum shrinks significantly for a given range of shades in the color bar. These observations on wave number-frequency power spectra of the T fluctuations are consistent with the intense uv events

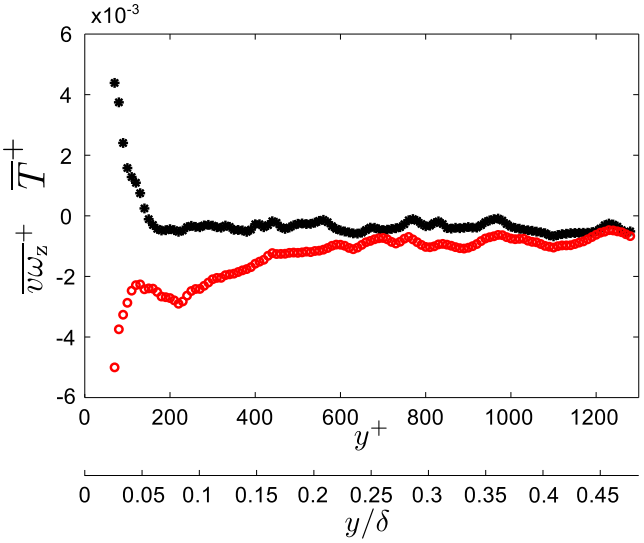

FIG. 1. Profile of $\overline{T}^+$ (black asterisks) and $\overline{v\omega_z}^+$ (red circles) at different wall-normal locations within the flow.

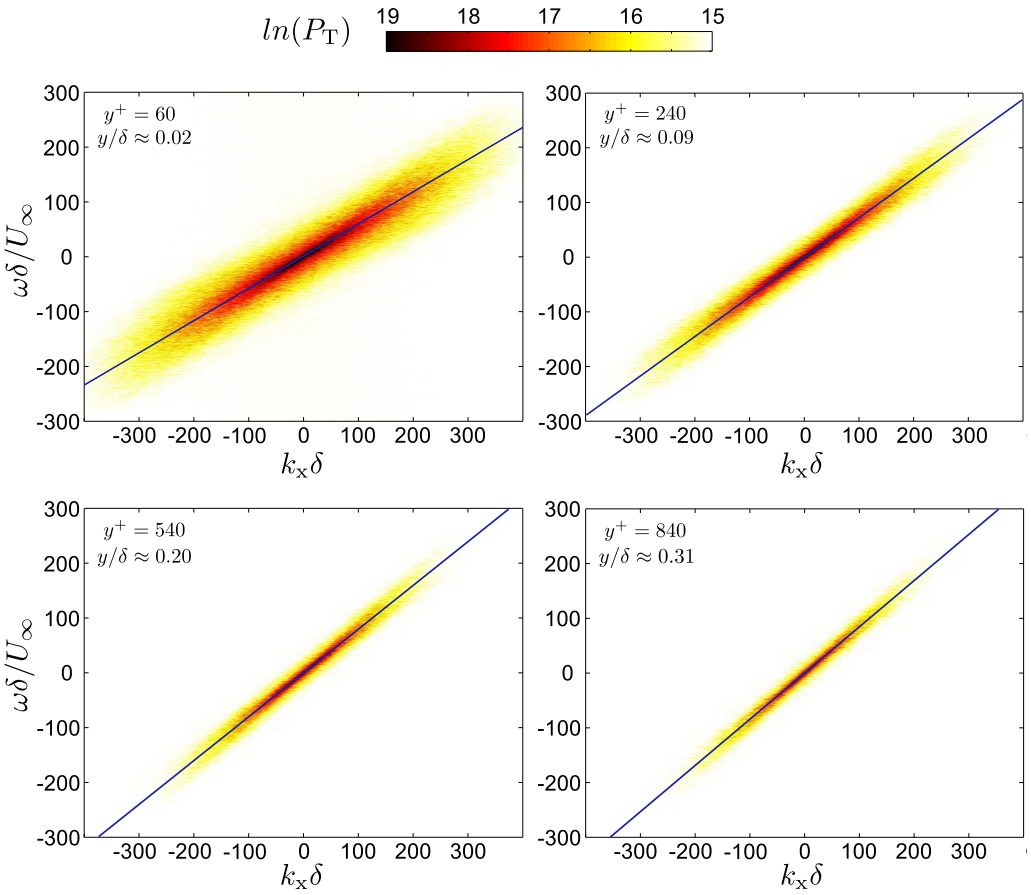

FIG. 2. Wave number-frequency power spectral density of the T fluctuations, at different wall-normal distances. Lines represent the local *mean* streamwise velocity.

being smaller in size and shorter in lifetime at the wall, which was postulated in the attached-eddy hypothesis in Ref. [32] and confirmed by recent hot-wire measurements [33] and time-resolved PIV data [28]. The described trend is more evident from Fig. 3, where power spectra of the T events are presented at the different wall-normal locations. These spectra were obtained from the wave number-frequency spectra shown in Fig. 2, by summing the spectral contributions of the different frequencies. From Fig. 3 it can be appreciated that the decrease in the spectral content for growing wall distances occurs similarly at every wave number of the spectrum. In other words, all the different spectra can be ideally obtained by vertically shifting the same spectrum. Moreover, from Fig. 3 it can be seen that the largest decrease in the spectral content of the T events occurs in proximity to the wall, thus when moving from $y^+ = 60$ to $y^+ = 140$. At increasing wall-normal locations, the drop in the spectral content becomes progressively less significant. As a result, the spectrum at $y^+ = 740$ and the spectrum at $y^+ = 1040$ nearly overlap.

From the wave number-frequency power spectra presented in Fig. 2, the local characteristic wave velocities (U_W) of momentum sources and sinks can be estimated and compared to the profile of mean streamwise velocities of the flow. For this purpose, a procedure analogous to Ref. [28] was established. Eight values of $\ln(P_T)$ at intervals of 0.25 were considered. Each value of $\ln(P_T)$ was taken as a contour level of the wave number-frequency power spectrum, and an ellipse was fitted to the points delimiting the edge of the contour level. A linear least-square fitting method was employed, which optimizes the squared sum of orthogonal distances from the points to the fitted ellipse. The

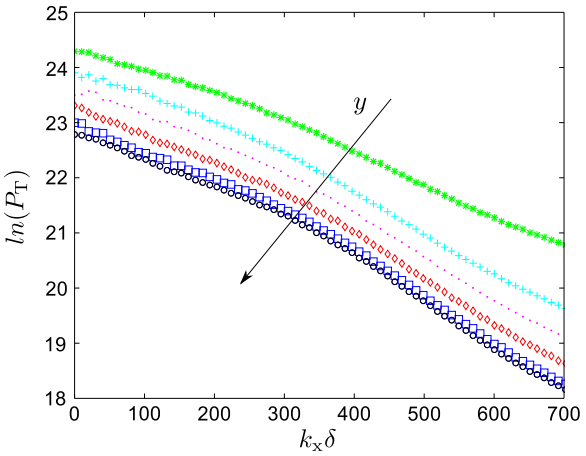

FIG. 3. Power spectra of T, at different wall-normal distances, ∗: $y^+ = 60$, +: $y^+ = 140$, •: $y^+ = 240$, ◊: $y^+ = 440$, □: $y^+ = 740$, ○: $y^+ = 1040$.

result of this procedure is presented in Fig. 4. As can be observed, the characteristic wave velocities approximately match the mean streamwise velocities of the flow for $\overline{U}/U_\infty < 0.8$. At larger distances from the wall, these wave velocities are mildly lower than the mean streamwise velocity of the flow. Overall, the characteristic wave velocities of the T events do not deviate significantly from the mean streamwise velocity of the flow. The deviations of the characteristic wave velocities of the T events from the mean streamwise flow velocities are analogous to the ones of the momentum transport events obtained by Ref. [28] (Fig. 5). This result confirms the statistical observations in Ref. [25], which found that at $y^+ = 110$ and at $y^+ = 575$ both momentum sources and sinks are correlated with low-momentum regions of the flow. It is worth stressing that the flow is never intermittent at the wall-normal locations object of the analysis given in Fig. 4, and the turbulent-nonturbulent interface is always located above that region (see Fig. 2 of Ref. [21]). We determine that the observed deviations of the wave velocities of momentum sources and sinks from the mean streamwise velocities cannot be explained as potential fluid at U_∞ contributing to the mean velocity profile.

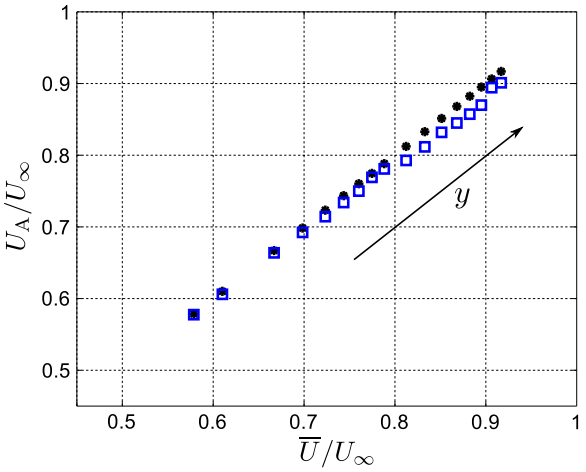

FIG. 4. Characteristic wave velocities of sources and sinks of momentum (blue squares) at different wall-normal locations, calculated from the wave number-frequency power spectra. Black filled spot indicates the mean streamwise velocity.

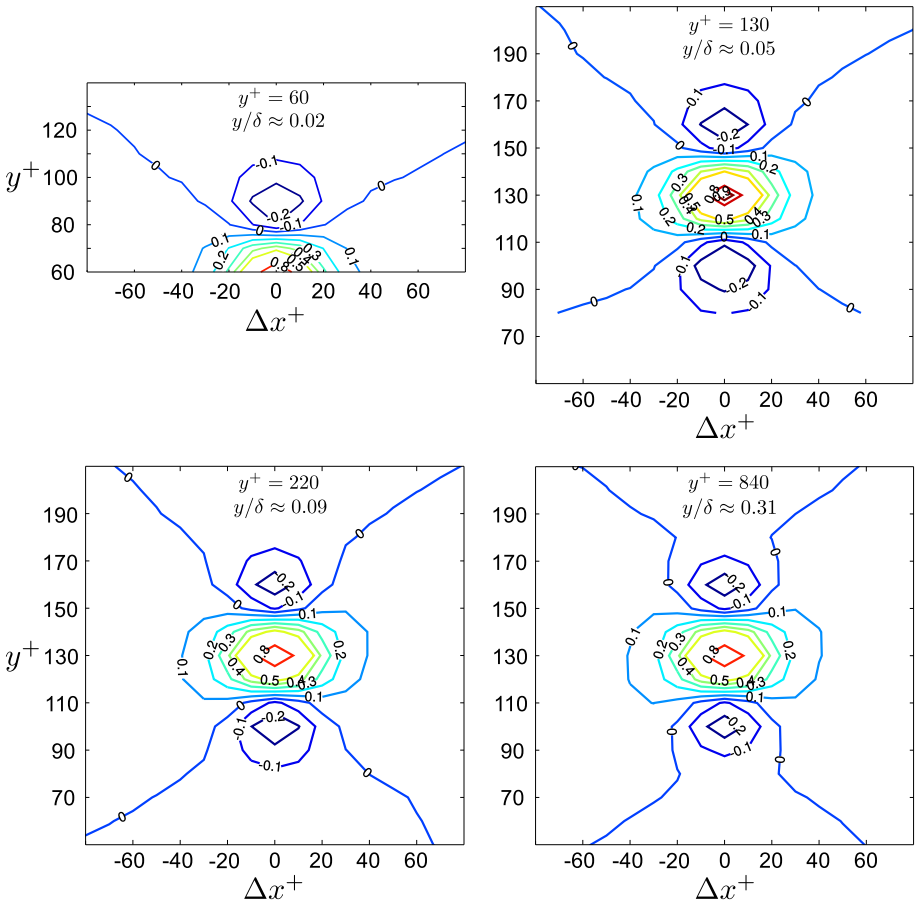

FIG. 5. Autocorrelation coefficient map of T events, at different wall-normal distances.

Following these observations, the wave number-frequency power spectra of the T fluctuations (Fig. 2) can be compared with spectra of the uv fluctuations, which were given in Fig. 4 of Ref. [28]. The two-peak structure that was identified in the spectra of the Reynolds-shear-stress fluctuations cannot be found when examining spectra of momentum sources and sinks. Considering that the two-peak structure of the spectra was interpreted as the result of two characteristic wave velocities, the absence of this structure in the T-fluctuation spectra indicates that only one single characteristic wave velocity exists for momentum sources and sinks, at a given wall-normal location. This seems to suggest that the streamwise wave velocities of these motions do not depend on the type of Reynolds-shear-stress (quadrant) events they are associated to. However, the characteristic wave velocities of T events and those of Reynolds-shear-stress events are comparable, as previously discussed.

It is of interest to examine the structure of the sources and sinks of momentum at different wall-normal locations. Specifically, geometrical properties of the T events such as size and shape can be statistically investigated based on autocorrelation coefficients maps. Each of these maps can be calculated by one-dimensional-correlating a T signal at a given distance from the wall with other T signals at different distances from the wall. The obtained map is normalized by the respective autocorrelation coefficient at a given wall distance, at zero shift. The result of this analysis can be observed in Fig. 5, where autocorrelation maps are presented at four different wall-normal locations: $y^+ = 60$ ($y/\delta \approx 0.02$), $y^+ = 130$ ($y/\delta \approx 0.05$), $y^+ = 220$ ($y/\delta \approx 0.09$), and $y^+ = 840$ ($y/\delta \approx 0.31$). As can be seen, the structure of the sources and sinks of momentum

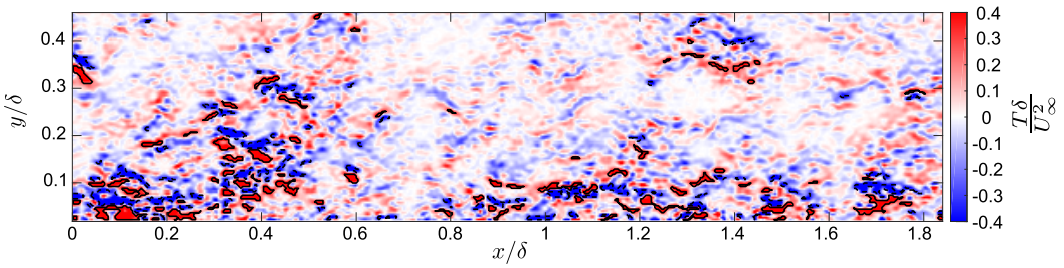

FIG. 6. Snapshot of sources and sinks of momentum. Black dashed lines mark intense momentum sinks, while black continuous lines mark intense momentum sources, both identified with the criterion shown in Eq. (5). Spots of different sizes and shades mark the time evolution of the weighted centroids of the intense events.

does not change significantly with the wall distance, and it is characterized by a nearly circular shape, slightly elongated along the streamwise direction.

The size structure of these events can be estimated as 60 wall units in the streamwise direction, and 40 wall units in the wall-normal direction, if $R = 0.2$ is adopted as a threshold. This result does not deviate significantly from the assessment of Ref. [25], which quantified the streamwise extent of T events with two-point correlations, at two different wall-normal locations, i.e., $y^+ = 110$ and $y^+ = 575$. At $y^+ = 110$, both momentum sources and sinks were quantified to be approximately 70 wall units along the x direction, while at $y^+ = 575$ momentum sources were quantified to be approximately 70 wall units and momentum sinks approximately 85 wall units [25]. Moreover, T events of opposite sign tend to be located in the close neighborhood of a T event, for a characteristic streamwise shift equal to zero ($\Delta x^+ \approx 0$), and at a characteristic wall-normal distance of around 30 wall units. It is worth underlining that the choice of providing the geometrical description of these motions in terms of wall units does not mean that their sizes scale as the inner units of the turbulent boundary layer. The scaling of these motions cannot be assessed based on only one single Reynolds number; therefore further investigations on turbulent boundary layers at a range of different Reynolds numbers would be necessary for this purpose.

The statistical observations thus far reported can be corroborated when watching the video "Movie1ssm.mov," which is part of the Supplemental Material [29]. The first frame of the video is given in Fig. 6. In this video, the intense sinks of momentum have been marked with a dashed black line, while the intense sources of momentum have been marked with a continuous line. It is worthy to recall that the criterion identifying an intense sink or source of momentum is given in Eq. (5). The video "Movie1ssm.mov" has been obtained from the same velocity vector fields as the video "Movie2.mov" included in Ref. [28], which presents the time evolution of the Q^- events. The time span covered in the video "Movie1ssm.mov" is $1.33\delta/U_\infty$, therefore the video reduces the flow velocity of approximately 150 times. The video "Movie1ssm.mov" shows that the sinks (blue) and sources (red) of momentum tend to be elongated in the streamwise direction, and that they are vertically bounded by events of opposite sign, consistent with the statistical findings based on autocorrelation and presented in Fig. 5. Therefore, the main evidence obtained from this video is that T events appear preferentially in pairs, and that they are typically stretched along the flow direction.

The described structure of the sources and sinks of momentum can be seen as a consequence of their mathematical definition. Across the external edge of an intense quadrant event, the absolute value of uv increases significantly with the wall distance (large $|\partial(-uv)/\partial y|$), which determines the identification of an intense T event. The internal side of the same bespoke edge is characterized by the opposite phenomenon, and the rapid drop of the absolute value of uv (large $|\partial(-uv)/\partial y|$) leads to the detection of an intense T event of the opposite sign. This gives an origin to the pairlike structure obtained statistically and shown in Fig. 5. The observed spatial organization can also be interpreted from a physical point of view. Turbulence acts as a balancer of momentum by redistributing the momentum surplus to the closest region where there is a momentum deficit and vice versa. The

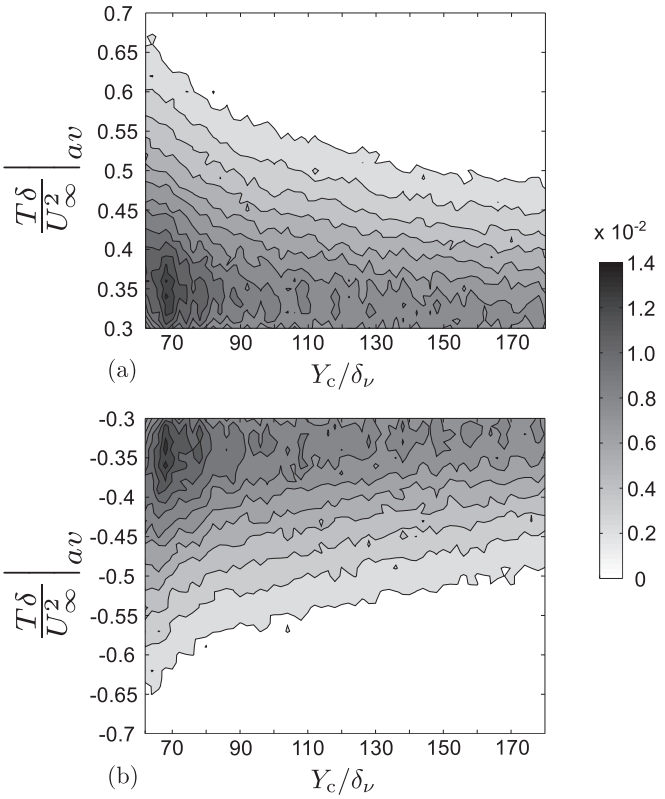

FIG. 7. Joint probability density function between the wall-normal locations of the positive (a) and negative (b) T events and their intensities averaged over the respective areas.

turbulent motions that actively play this role are momentum sources and sinks [Eq. (1)]. As a result of this process, turbulence levels off the mean velocity profile of a TBL when compared to a laminar boundary layer. From the size structure of Fig. 5 it can be observed that the described redistribution is a local small-scale phenomenon, even though it results ultimately in a flattened mean velocity profile, which is a macroscopic effect. Therefore, the small scales of turbulence seem to be the main factors responsible for flattening the mean velocity profile in turbulent wall-bounded flows. This conclusion could be interpreted as in contradiction with the mean velocity profile being accurately captured in large-eddy simulations (LESs), where the small scales of turbulence are not directly resolved but only modeled. However, it could be that the stochastic behavior of momentum sources and sinks can be captured in the mean sense from LESs, but LESs fail to capture these motions instantaneously.

The detected intense sources and sinks of momentum can be described based on their average intensity and wall-normal position within the flow. In Fig. 7 the joint probability density function (JPDF) between the intensity and the wall distance of the intense momentum sources (top) and sinks (bottom) is presented. The largest number of T events is detected close to the wall, while at increasing wall-normal locations the probability of finding them diminishes. This is consistent with the observations of Refs. [33] and [28]. Both experimental investigations reported a decreasing number of intense *uv* events when moving away from the wall, which implies that a lower number of momentum sources and sinks can also be detected for growing wall-normal locations. From Fig. 7 we can observe that in proximity to the wall, we have the largest range of intensities. This range tends to become more and more narrow at growing wall-normal locations. The two JPDFs look almost specular, even though in proximity to the wall there is a larger probability to find a momentum source than a momentum sink. This is consistent with the mean T profile across the TBL (Fig. 1).

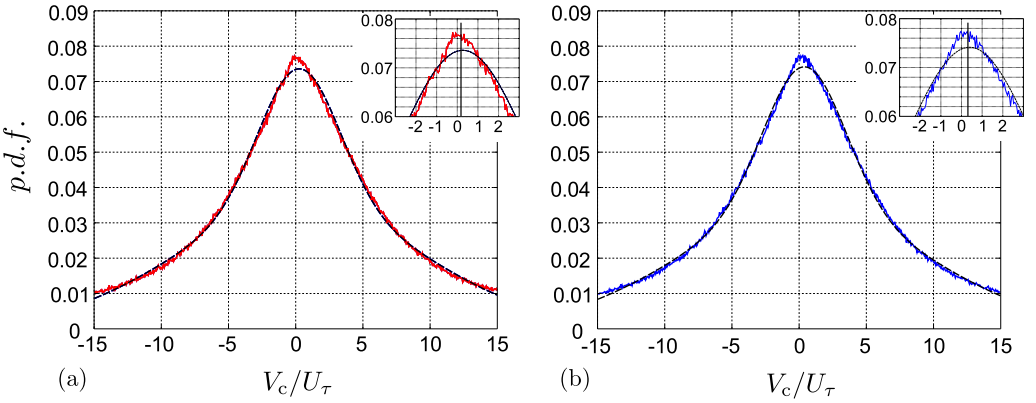

FIG. 8. Probability density functions of the wall-normal component of the local velocities (V_c) of the intense momentum sources (a) and sinks (b) (continuous line) and a two-term Gaussian fitting curve (dashed line). The vertical lines in the insets represent the *mean* values, which are respectively of 0.20 for the momentum sources and of 0.25 for the momentum sinks.

From the tracking in time of the T events we can estimate their local velocities. Figure 8 shows the probability density functions (PDFs) of the wall-normal component of the local velocities (V_c) of the intense momentum sources and sinks. Two-term Gaussian fitting curves have been added to the PDFs and drawn with a dashed line. It can be observed that the distribution of the vertical velocities is nearly Gaussian for both positive and negative T events. From the two PDFs it is difficult to confidently determine the position of the peak values of the two PDFs. If we look at the peak value of the fitting curves, we can observe that they are both located in the positive part of the graph. Consistent with this result, the mean of the vertical velocities of both sources and sinks calculated from the range $-15 < V_c/U_\tau < 15$ gives $V_c/U_\tau = 0.20$ for momentum sources, and $V_c/U_\tau = 0.25$ for momentum sinks. These values have been marked with vertical black lines in the insets of Fig. 8. Therefore, T events have the tendency to move upwards, at a vertical velocity that is a small fraction of the friction velocity, U_τ. This finding reinforces the results obtained in Ref. [25], in which it is reported that at $y^+ = 110$ and at $y^+ = 575$ both momentum sources and sinks are correlated with regions of upwash.

It is worth noting that, in consequence of splitting of events across time, one event at a certain time instant can be associated with two or more events at the following time instant, thus leading to two or more local velocities. In this respect, all the local velocities obtained from time tracking intense transport events contributed to the statistics presented in the following. Furthermore, the wall-normal location associated with a certain displacement (and thus local velocity) is the wall-normal location of the weighted centroid of the forward tracked intense event by convention.

Perhaps of more interest is to examine the streamwise component of the local velocities of the T events (U_c) obtained from their tracking in time, and to compare these local velocities to the wave velocities estimated from the analysis of the spectra (Fig. 2). The joint probability density functions between the local streamwise velocities and the wall-normal locations of the momentum sources (left) and sinks (right) are given in Fig. 9. The blue dashed lines represent the mean streamwise velocity of the flow, and the two black thick lines in each JPDF identify a region where the number of samples of U_c is larger than 50% of the largest number of samples at a given wall-normal location. Asterisks mark the mean values of the local streamwise velocities of momentum sources and sinks at different wall-normal locations. As can be observed, the two JPDFs are very similar. This is evidence that the sign of the T events does not affect significantly the distribution of their local velocities U_c at different wall-normal positions. In the JPDFs, the isoprobability contours widen at decreasing wall-normal locations, therefore as the wall approaches. This is a consequence of the largest number of intense momentum sources and sinks being identified in proximity to the wall. From the mean of the local

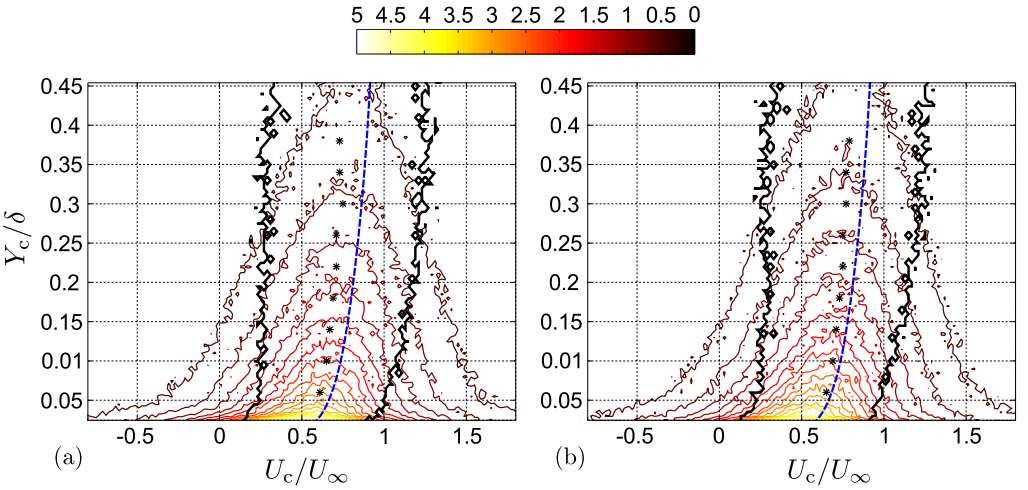

FIG. 9. Joint probability density functions between the streamwise component of the local velocities (U_c) of the positive (a) and negative (b) T events and their wall-normal locations (Y_c). The black thicker line is a contour of the 50% of the peak value at each wall-normal location. The blue dashed line represents the streamwise component of the mean velocity profile of the flow ($\overline{U}/U_\infty$). Asterisks ($*$) mark the mean of the local streamwise velocities of the intense T events.

streawise velocites (marked with the asterisks) and from the area delimited by two black thick lines, it appears that the T events are characterized by local streamwise velocities mildly lower than the mean flow velocity, and that this velocity difference increases with the wall distance. This is consistent with the estimate of the characteristic wave velocities from the analysis of the spectra (see Fig. 4).

In the upper range of the logarithmic region and in the wake region of turbulent boundary layers and channel flows, the small-scale motions were observed in the past to be characterized by convection velocities lower than the mean streamwise velocity (see Fig. 8 of Ref. [34], Fig. 21 of Ref. [2], and Fig. 2 of Ref. [35]). Given that sources and sinks of momentum can be considered small-scale motions (Fig. 5), the results obtained in the present work confirm those observations.

IV. CONCLUSIONS

The characteristics of sources and sinks of momentum in space-time and wave number-frequency domains were examined in a turbulent boundary layer ($\mathrm{Re}_\tau = 2700$), using time-resolved PIV data in a plane along the streamwise and wall-normal directions. The field of view in the PIV measurements covers a range of wall-normal locations from 50 to 1280 wall units, which is equivalent to $y/\delta \approx 0.46$.

The mean profile of the Reynolds stress gradient, identified as T throughout the paper, shows a monotonic decrease in the range between 50 and 160 wall units. At $y^+ \approx 140$, the Reynolds stress gradient becomes negative, and it remains negative at increasing wall distances. This indicates that in proximity to the wall there is a prevalence of momentum sources, while momentum sinks tend to be dominant farther away from the wall, consistent with the average profile of Reynolds shear stress. The spectral composition of momentum sources and sinks was quantified from the wave number-frequency power spectra of T fluctuations. The larger spectral content was obtained at the lowest wall-normal location available from measurement, while at increasing wall distance the spectral content decreases. The distribution of spectral contents among the different wave numbers (and therefore wavelengths) remains approximately the same at the different wall-normal locations under analysis. The two-peak structure that was identified in the wave number-frequency spectra of the Reynolds-shear-stress fluctuations [28] cannot be detected in the current study when examining spectra of

momentum sources and sinks. From this it seems that the streamwise wave velocities of these motions do not depend on the type of Reynolds-shear-stress (quadrant) events they are associated to.

Wave number-frequency power spectra enabled to estimate the wave velocities of the T fluctuations at different wall distances. A procedure analogous to that of Ref. [28] was applied. It was found that the characteristic wave velocities of the T events approximately match the local streamwise velocities of the flow ($\overline{U}$) near the wall (for $\overline{U}/U_\infty < 0.8$). At larger distances from the wall, the characteristic wave velocities are slightly lower than the local streamwise velocity of the flow. Analogous observation was obtained from time tracking of the intense T events. This finding is consistent with sources and sinks of momentum being preferentially located in low-speed regions of the flow, as the authors of Ref. [25] found in a turbulent boundary layer, at $y^+ = 110$ and at $y^+ = 575$.

Size and spatial organization of momentum sources and sinks were investigated with autocorrelation coefficient maps. The spatial extent of the T events along the streamwise and wall-normal directions can be estimated as 60 and 40 wall units, respectively, and it does not change significantly with the wall distance. Furthermore, T events of opposite sign can be found in the close neighborhood of a T event, at a characteristic streamwise shift approximately equal to zero ($\Delta x^+ \approx 0$), and a characteristic wall-normal distance of around 30 wall units. This finding was confirmed from instantaneous visualizations of contour maps of T events. It was observed that momentum sources and sinks appear preferentially in pairs, and that their shape is elongated along the flow direction.

ACKNOWLEDGMENTS

The authors acknowledge the financial support of the European Research Council (ERC Grant No. 277472) and the Engineering and Physical Sciences Research Council of the United Kingdom (EPSRC Grant No. EP/L006383/1).

[1] R. J. Adrian, Hairpin vortex organization in wall turbulence, Phys. Fluids **19**, 041301 (2007).
[2] R. J. Adrian, C. D. Meinhart, and C. D. Tomkins, Vortex organization in the outer region of the turbulent boundary layer, J. Fluid Mech. **422**, 1 (2000).
[3] R. J. Adrian and Z.-C. Liu, Observation of vortex packets in direct numerical simulation of fully turbulent channel flow, J. Visualiz. **5**, 9 (2002).
[4] B. Ganapathisubramani, E. K. Longmire, and I. Marusic, Characteristics of vortex packets in turbulent boundary layers, J. Fluid Mech. **478**, 35 (2003).
[5] A. Lozano-Duran, O. Flores, and J. Jimenez, The three-dimensional structure of momentum transfer in turbulent channels, J. Fluid Mech. **694**, 100 (2012).
[6] A. Lozano-Duran and J. Jimenez, Time-resolved evolution of coherent structures in turbulent channels: Characterization of eddies and cascades, J. Fluid Mech. **759**, 432 (2014).
[7] N. Hutchins and I. Marusic, Evidence of very long meandering features in the logarithmic region of turbulent boundary layers, J. Fluid Mech. **579**, 1 (2007).
[8] D. Chung and B. J. McKeon, Large-eddy simulation of large-scale structures in long channel flow, J. Fluid Mech. **661**, 341 (2010).
[9] J. H. Lee and H. J. Sung, Very-large-scale motions in a turbulent boundary layer, J. Fluid Mech. **673**, 80 (2011).
[10] L. H. O. Hellström, B. Ganapathisubramani, and A. J. Smits, The evolution of large-scale motions in turbulent pipe flow, J. Fluid Mech. **779**, 701 (2015).
[11] T. Wei, P. Fife, J. C. Klewicki, and P. McMurtry, Properties of mean momentum balance in turbulent boundary layer, channel and pipe flows, J. Fluid Mech. **522**, 303 (2005).
[12] P. Fife, T. Wei, J. C. Klewicki, and P. McMurtry, Stress gradient balance layers and scale hierarchies in wall bounded turbulent flows, J. Fluid Mech. **532**, 165 (2005).
[13] J. C. Klewicki, P. Fife, T. Wei, and P. McMurtry, A physical model of the turbulent boundary layer consonant with mean momentum balance structure, Phil. Trans. R. Soc. A **365**, 823 (2007).

[14] J. O. Hinze, *Turblence* (McGraw-Hill, New York, 1975).
[15] J. C. Klewicki, Velocity-vorticity correlations related to the gradients of the Reynolds stresses in parallel turbulent wall flows, Phys. Fluids **1**, 1285 (1989).
[16] A. L. Rovelstad, Lagrangian analysis of vorticity transport in a numerically simulated turbulent channel flow, Ph.D. thesis, University of Maryland, 1991.
[17] L. Ong, Visualization of turbulent flows with simultaneous velocity and vorticity measurements, Ph.D. thesis. University of Maryland, 1992.
[18] A. L. Rajagopalan and R. A. Antonia, Structure of the velocity field associated with the spanwise vorticity in the wall region of a turbulent boundary layer, Phys. Fluids **5**, 2502 (1993).
[19] J. C. Klewicki, J. A. Murray, and R. E. Falco, Vortical motion contributions to stress transport in turbulent boundary layers, Phys. Fluids **6**, 277 (1994).
[20] P. J. A. Priyadarshana, J. C. Klewicki, S. Treat, and J. Foss, Statistical structure of turbulent-boundary-layer velocity-vorticity products at high and low Reynolds numbers, J. Fluid Mech. **570**, 307 (2007).
[21] J. Eisma, J. Westerweel, G. Ooms, and G. Elsinga, Interfaces and internal layers in a turbulent boundary layer, Phys. Fluids **27**, 055103 (2015).
[22] C. M. Silva, N. Hutchins, and I. Marusic, Uniform momentum zones in turbulent boundary layers, J. Fluid Mech. **786**, 309 (2016).
[23] M. Guala, S. E. Hommema, and R. J. Adrian, Large-scale and very-large-scale motions in turbulent pipe flow, J. Fluid Mech. **554**, 521 (2006).
[24] J. P. Monty, J. C. Klewicki, and B. Ganapathisubramani, Characteristics of momentum sources and sinks in turbulent channel flow, in *Proceedings of the 7th International Symposium on Turbulence and Shear Flow Phenomena*, Ottawa, Canada, July 28–31, 2011.
[25] B. Ganapathisubramani, Statistical structure of momentum sources and sinks in the outer region of a turbulent boundary layer, J. Fluid Mech. **606**, 225 (2008).
[26] W. W. Willmarth and S. S. Lu, Structure of the Reynolds stress near the wall, J. Fluid Mech. **55**, 65 (1972).
[27] R. dea Kat and B. Ganapathisubramani, Frequency-wavenumber mapping in turbulent shear flows, J. Fluid Mech. **783**, 166 (2015).
[28] D. Fiscaletti, R. dea Kat, and B. Ganapathisubramani, Spatial-spectral characteristics of momentum transport in a turbulent boundary layer, J. Fluid Mech. **836**, 599 (2018).
[29] See Supplemental Material at http://link.aps.org/supplemental/10.1103/PhysRevFluids.3.054601 for video Movie 1ssm.mov, and http://doi.org/10.5258/SOTON/D0297 for the data set used in this paper.
[30] G. Elsinga, R. J. Adrian, B. vana Oudheusden, and F. Scarano, Three-dimensional vortex organization in a high-Reynolds-number supersonic turbulent boundary layer, J. Fluid Mech. **644**, 35 (2010).
[31] R. J. Adrian and J. Westerweel, *Particle Image Velocimetry* (Cambridge University Press, Cambridge, 2011).
[32] A. Townsend, Equilibrium layers and wall turbulence, J. Fluid Mech. **11**, 97 (1961).
[33] C. Morrill-Winter, J. Philip, and J. Klewicki, Statistical evidence of an asymptotic geometric structure to the momentum transporting motions in turbulent boundary layers, Phil. Trans. R. Soc. A **375**, 20160084 (2017).
[34] R. Mathis, N. Hutchins, and I. Marusic, Large-scale amplitude modulation of the small-scale structures in turbulent boundary layers, J. Fluid Mech. **628**, 311 (2009).
[35] J. C. del Álamo and J. Jiménez, Estimation of turbulent convection velocities and corrections to Taylor's approximation, J. Fluid Mech. **640**, 5 (2009).